Editors' Suggestion

Robust Nuclear Spin Polarization via Ground-State Level Anticrossing of Boron Vacancy Defects in Hexagonal Boron Nitride

Shihao Ru,[1,*] Zhengzhi Jiang,[2,3,*] Haidong Liang,[4,*] Jonathan Kenny,[1,*] Hongbing Cai,[1,5] Xiaodan Lyu,[1,5] Robert Cernansky,[6] Feifei Zhou,[7,1] Yuzhe Yang,[1] Kenji Watanabe,[8] Takashi Taniguch,[8] Fuli Li,[9] Teck Seng Koh,[1] Xiaogang Liu,[2,3] Fedor Jelezko,[6,†] Andrew A. Bettiol,[4,‡] and Weibo Gao[1,5,10,§]

[1]*Division of Physics and Applied Physics, School of Physical and Mathematical Sciences, Nanyang Technological University, Singapore 637371, Singapore*

[2]*Department of Chemistry, National University of Singapore, Singapore 117543, Singapore*

[3]*Joint School of National University of Singapore and Tianjin University, International Campus of Tianjin University, Binhai New City, Fuzhou 350207, P. R. China*

[4]*Centre for Ion Beam Applications, Department of Physics, National University of Singapore, Singapore 117542, Singapore*

[5]*The Photonics Institute and Centre for Disruptive Photonic Technologies, Nanyang Technological University, Singapore 637371, Singapore*

[6]*Institute for Quantum Optics and Centre for Integrated Quantum Science and technology (IQST), Ulm University, Albert-Einstein-Allee 11, 89081 Ulm, Germany*

[7]*College of Metrology Measurement and Instrumentation, China Jiliang University, Hangzhou, 310018, China*

[8]*International Center for Materials Nanoarchitectonics, National Institute for Materials Science, Tsukuba 305-0044, Japan*

[9]*School of Physics, Xi'an Jiaotong University, Xi'an 710049, China*

[10]*Centre for Quantum Technologies, National University of Singapore, Singapore 117543, Singapore*

(Received 28 June 2023; revised 23 December 2023; accepted 30 May 2024; published 24 June 2024)

Nuclear spin polarization plays a crucial role in quantum information processing and quantum sensing. In this work, we demonstrate a robust and efficient method for nuclear spin polarization with boron vacancy (V_B^-) defects in hexagonal boron nitride (h-BN) using ground-state level anticrossing (GSLAC). We show that GSLAC-assisted nuclear polarization can be achieved with significantly lower laser power than excited-state level anticrossing, making the process experimentally more viable. Furthermore, we have demonstrated direct optical readout of nuclear spins for V_B^- in h-BN. Our findings suggest that GSLAC is a promising technique for the precise control and manipulation of nuclear spins in V_B^- defects in h-BN.

DOI: 10.1103/PhysRevLett.132.266801

Optically addressable solid-state spin defects in wide band-gap materials serve as promising artificial atoms for quantum information sciences. For instance, spin defects in diamond and silicon carbide exhibit long spin coherence times, high-fidelity spin manipulations, and entangled electron-nuclear spin pairs at room temperature [1–6]. In addition, layered Van der Waals materials offer alternative platforms for solid-state spin defects, with reduced dimensionality facilitating scalable two-dimensional quantum device design. Among them, hexagonal boron nitride (h-BN) has attracted significant interest due to its exceptional properties, such as wide band gap, high thermal conductivity, and robust mechanical strength [7]. Recently, negatively charged boron vacancy (V_B^-) defects in h-BN have been extensively studied for their coherently manipulatable spin states and high optically detected magnetic resonance (ODMR) contrast at room temperature [8,9], critical for sensitivity in quantum sensing applications [10–15]. Polarization and rapid manipulation of adjacent nitrogen nuclear spins in h-BN via excited-state level anticrossing (ESLAC) have been achieved [16], offering avenues to store and manipulate quantum information [17,18].

The ESLAC approach to nuclear spin polarization in h-BN has limitations, such as the need for high excitation laser power and low levels of nuclear spin polarization [19–22]. To address the challenge, we investigate the use of ground-state level anticrossing (GSLAC) of V_B^- for achieving nuclear spin polarization in h-BN. GSLAC provides several advantages over ESLAC, including increased robustness against excitation laser power fluctuations and higher nuclear spin polarization level. In this Letter, we present an in-depth study of the GSLAC method and demonstrate its potential for enhancing the performance of nuclear spin polarization in V_B^- systems [16,19,23]. We initiate our study by evaluating the levels of nuclear polarization at ESLAC and GSLAC regions. Our findings suggest that, even under comparatively low excitation power, GSLAC can induce high levels of nuclear polarization. Then we measure the nuclear polarization level as a function of magnetic field, aiming to find the optimal

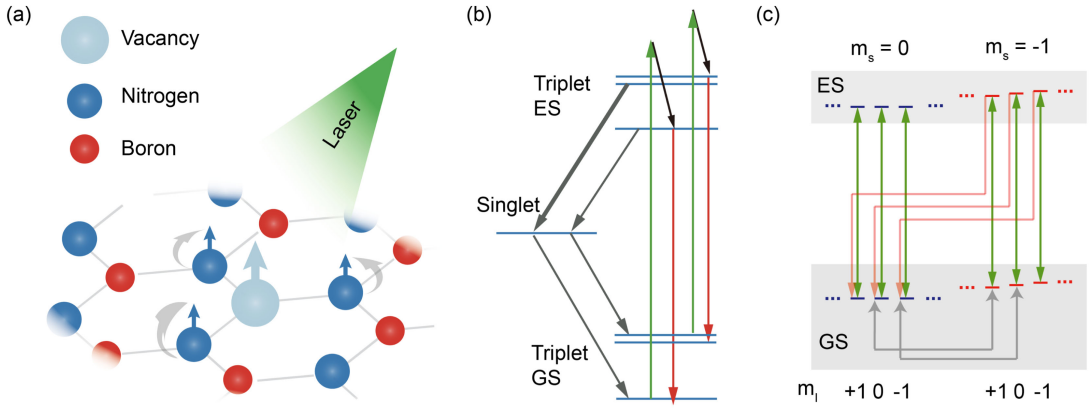

FIG. 1. (a) Scheme for performing nuclear polarization with the assistance of GSLAC. Magnetic field is not shown. (b) Diagram of energy levels of V_B^- with optical transitions. Green, red, and gray arrows represent laser excitation, radiative recombination, and nonradiative intersystem crossing, respectively. (c) Simplified diagram of dynamics of nuclear polarization via GSLAC. Excitation and radiative decay are depicted by green arrows, while red arrows show electron spin polarization through intersystem crossing. Gray arrows illustrate flip-flop process. For simplicity, more energy levels and transitions are omitted.

nuclear polarization level. Lastly, we have demonstrated the direct optical readout of nuclear spins through optically detected nuclear magnetic resonance (ODNMR). These comprehensive experimental endeavors pave the way for advancing quantum information processing, enhancing nuclear magnetic resonance spectroscopy sensitivity, and enabling the development of high-performance nuclear spin-based sensors.

Boron vacancy and its energy levels.—The V_B^- defect in h-BN is a point defect that occurs when a boron atom is missing from the crystal lattice, as shown in Fig. 1(a) [8]. A V_B^- defect has a triplet ground state, a triplet excited state, and a nonradiative singlet metastable state. When illuminated with a green laser, V_B^- defects are optically excited from the ground state to the excited state. The defects can then undergo spin-dependent intersystem crossing (ISC) to the singlet metastable state, leading to spin polarization. The spin-dependent nature of the ISC processes also results in spin-dependent fluorescence, enabling optical detection and manipulation of the V_B^- defect's spin state. The dynamics is shown in Fig. 1(b) [24].

Nuclear polarization assisted by GSLAC.—As the external magnetic field is tuned, the energy levels of $m_s = 0$ and $m_s = -1$ states become nearly degenerate at certain magnetic field values, leading to level anticrossing [8,16,19,25]. At these points, the wave functions of the electronic and nuclear spin states mix, allowing for a strong interaction between them. Through this interaction, the electronic and nuclear spins can exchange spin angular momentum. This can be facilitated by a process called flip flop, where the electronic spin flips while the nuclear spin flops simultaneously in the opposite direction. A diagram of dynamics of nuclear polarization assisted by GSLAC is shown in Fig. 1(c). The flip-flop process is indicated by gray arrows. As a result, the spin polarization of the electronic spin is transferred to the nuclear spins, enhancing their polarization.

Sample preparation and setup.—h-BN flakes with thickness of several μm were proton bombarded at 250 keV energy and 3×10^{16} cm^{-2} dose to create dense V_B^- defects [26]. A homemade confocal microscope was used in the experiment. A $40 \times /0.6$ visible objective focused the excitation laser onto the sample and collected fluorescence. A 532 nm laser modulated by an acoustic optical modulator provided off-resonance excitation. The photoluminescence signal, filtered through a 700-nm long pass and 1000-nm short pass filter, was coupled to a photodiode. The microwave generated by an rf signal generator and gated by an rf switch, was amplified, and applied to the sample via a coplanar waveguide where the h-BN flake was placed. A permanent magnet on a three-axis motorized translation stage provided the magnetic field. Magnetic field alignment along the sample's c axis was done before the experiment [27].

Extraction of populations of nuclear spin states.—For V_B^- defects, the hyperfine interactions between the central electron spin and the three nearest nitrogen nuclear spins cause each electronic state to split into 7 sublevels. This results in an ODMR peak that consists of 7 subpeaks, separated by a hyperfine value of approximately 47 MHz [8,16]. To analyze the population of the nuclear spin states, the ODMR results are fitted with 7 peaks corresponding to these sublevels. By fitting the ODMR results with 7 subpeaks, we can extract the area of each subpeak, which is proportional to the population of the corresponding nuclear spin state [16,19]. This allows us to determine the nuclear spin polarization in the V_B^- system and further analyze the effectiveness of the GSLAC and ESLAC techniques for achieving nuclear spin polarization.

Laser power dependence in ESLAC and GSLAC: A comparative study.—The laser power requirements for the

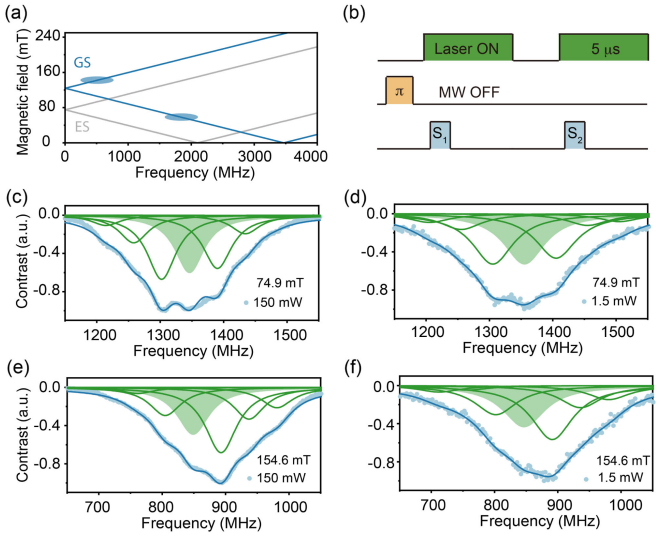

FIG. 2. (a) A diagram depicting the ODMR of V_B^- defects under an external magnetic field aligned with the c axis. The bottom and top shaded regions correspond to the magnetic fields of (c),(d) and (e),(f), respectively. (b) The pulse sequence used for pulsed ODMR measurement, featuring crucial parameters labeled accordingly. The laser, microwave, and readout window are arranged from top to bottom, respectively. (c),(d) Pulsed ODMR spectra captured at the magnetic field indicated by the bottom shaded area in (a), with laser powers of 150 (c) and 1.5 mW (d). The ODMR of $m_I = 0$ is highlighted by green shaded areas for easy reference. (e),(f) Pulsed ODMR spectra captured at the magnetic field indicated by the top shaded area in (a), replicating the conditions in (c),(d).

ESLAC and GSLAC methods in achieving nuclear spin polarization can be studied with pulsed ODMR spectra. Pulsed ODMR measurements are conducted at magnetic fields indicated by the shaded areas in Fig. 2(a). The lower and upper shaded fields correspond to the regions near ESLAC and GSLAC, respectively. The implemented measurement sequence is outlined in Fig. 2(b). We define the contrast of pulsed ODMR as $(S_1 - S_2)/(S_1 + S_2)$.

Pulsed ODMR results near the ESLAC region (74.9 mT) are analyzed with two laser powers: 150 mW [Fig. 2(c)] and 1.5 mW [Fig. 2(d)]. We employ the formula,

$$P_{\text{nuclear}} = \left(\sum m_I A_I\right) / \left(3 \sum A_I\right), \tag{1}$$

to quantitatively compute the nuclear polarization levels, where m_I is the quantum number of nuclear spin state and A_I is the area of subpeak of m_I nuclear spin state. We observe nuclear polarization levels of 0.0655 ± 0.008 and 0.0343 ± 0.024 for 150 and 1.5 mW, respectively. The relatively lower polarization at 1.5 mW suggests that ESLAC demands high laser power for increasing nuclear spin polarization, even though still in a modest level. In contrast, pulsed ODMR results near the GSLAC region (154.6 mT) are depicted in Figs. 2(e) and 2(f) for laser powers of 150 and 1.5 mW, respectively. Both measurements exhibit high nuclear polarization, with levels of 0.225 ± 0.006 and 0.170 ± 0.023 for 150 and 1.5 mW, respectively. These results underscore the efficiency of GSLAC in achieving substantial nuclear spin polarization in h-BN systems, even at lower excitation laser power, compared to ESLAC. This characteristic renders GSLAC more advantageous for practical applications where low-power operation is desired.

The robustness of GSLAC-assisted nuclear polarization is attributed to the longer residence time in the ground state prior to excitation due to light absorption. The nuclear polarization process entails two steps: initial electron spin polarization through spin-dependent ISC under laser illumination, followed by transfer of this polarization to the nuclear spins. The transfer occurs due to the precession of superposition states, either at the excited states (ESLAC) or the ground states (GSLAC) [19]. A shorter residence time, such as the excited state lifetime of about 1.258 ns at room temperature (refer to [27]), restricts the duration for the flip-flop process to occur. This results in the system rapidly reverting to the ground state, thus curtailing the nuclear polarization level achievable at low pump power.

Optimization of nuclear polarization.—To identify the magnetic field range that yields the highest nuclear polarization level, we assessed the nuclear polarization levels over a magnetic field range spanning from 25 to 200 mT. This span encapsulates both the ESLAC and GSLAC regions. It is important to note that the data corresponding to the precise GSLAC point, occurring around 133 mT in Fig. 3, could not be obtained from ODMR spectra due to significant spin state mixing. To accelerate the measurements and obtain reliable estimates for nuclear polarization levels, we opted for continuous wave (cw) ODMR, which provides superior signal-to-noise ratio. It should be stressed that, within the ESLAC region, cw ODMR enables greater nuclear polarization levels compared to pulsed ODMR, because of the higher average laser power.

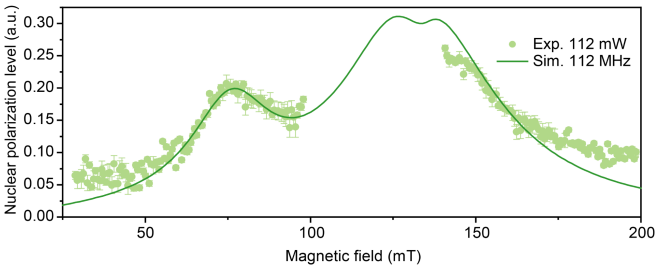

FIG. 3. The degree of nuclear spin polarization obtained from CW ODMR spectra is plotted against magnetic field in the range of 28 to 200 mT. The experimental results are represented by dots, while theoretical results are presented using curves. Laser power used in experiments and pump rate used in simulations have been labeled.

The collected data, pertaining to a laser power of 112 mW, are depicted as green dots in Fig. 3. Upon the gradual increment of the magnetic field to 74.9 mT (ESLAC), we observed a peak in the nuclear polarization level. Subsequently, as the magnetic field continued to increase, the polarization level initially decreased, only to start rising again upon entering the GSLAC region. The polarization level exhibits a gradual decline beyond the GSLAC point and this trend persists with further elevation in the magnetic field. The highest nuclear polarization level observed experimentally, 0.262 ± 0.005, manifests around 141 mT. This magnetic field is the closest measurable point to the GSLAC in our experimental field range.

To estimate the nuclear polarization within the region near the GSLAC (100 to 140 mT), where experimental data could not be obtained, we performed a theoretical simulation. We model the system with a Hamiltonian, consisting of an electronic spin (V_B^-) and three adjacent nitrogen nuclear spins [16,27]. The population of each state is extracted after arbitrarily long laser interaction to ensure that a steady state is reached. To get the levels of nuclear polarization at the strong mixing range, we extract the population of each m_I state from the simulation results. The nuclear polarization levels calculated as a function of magnetic field are depicted as a green curve in Fig. 3. In our simulation, the nuclear polarization peaks at a level of 0.311, occurring near a magnetic field strength of 127 mT. The nuclear polarization levels predicted by our simulation align well with our experimental results within the measurable ranges, underscoring the reliability of our model [39].

It is important to note that the observed relatively low nuclear polarization level can be attributed to the unequal hyperfine interaction components, A_{xx} and A_{yy}. These elements contribute to the nondiagonal hyperfine Hamiltonian, which promotes not only zero-quantum transitions but also two-quantum transitions in the vicinity of the level anticrossing [40,41]. Unlike in NV centers, this leads to unprotected highest quantum states in boron vacancies, $|m_s = 0, m_{I\,\mathrm{total}} = +3\rangle$, affecting nuclear polarization. Our simulations, depicted in Fig. S13, support this, showing higher polarization with equal hyperfine components. Future research could beneficially focus on strain engineering as a method to adjust the A_{xx} and A_{yy} hyperfine components, potentially leading to greater polarization levels [27].

Optically detected nuclear magnetic resonance.—The nuclear polarization induced by flip flop can lead to the direct optical readout of nuclear spins. When only zero-quantum transitions are considered $|m_s = 0, m_{I_1,I_2,I_3} = +1, +1, +1\rangle$, gives the largest fluorescence signal in general because it did not go through the flip-flop transition. (any flip of nuclear spins will lead to $|m_s = +1\rangle$, which has different energy level with $|m_s = 0\rangle$, and therefor no mixing is happening). Other states, for instance, $|m_s = 0, m_{I_1,I_2,I_3} = 0, +1, +1\rangle$ can mix with $|m_s = -1, m_{I_1,I_2,I_3} = +1, +1, +1\rangle$, which subsequently transits to a dark state via ISC. Therefore, this reduces the fluorescence from such states since it goes through the dark state. This mechanism will allow us to read the nuclear state directly with sequence as shown in Figs. 4(a) and 4(b), an approach as ODNMR. The role of two-quantum transitions on ODNMR is discussed in the Ref. [27].

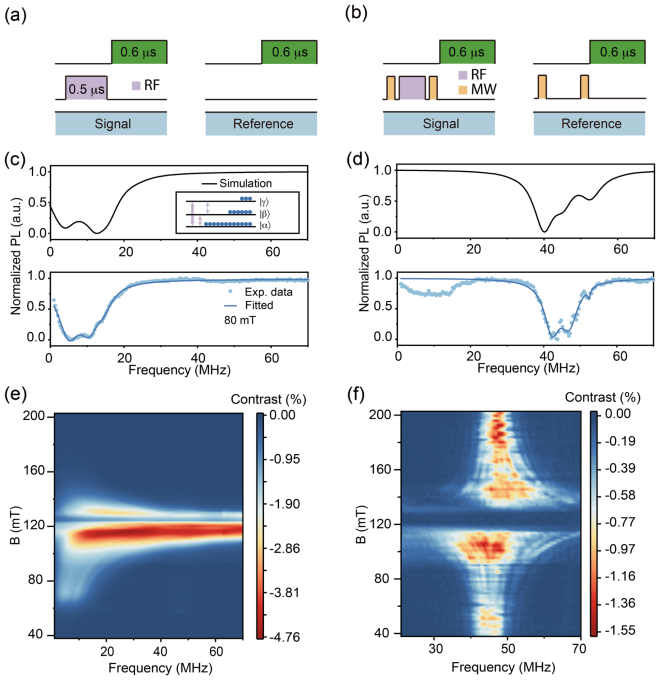

FIG. 4. (a),(b) Pulse sequence of ODNMR measurements for $m_s = 0$ (a) and $m_s = -1$ (b) branches. The laser, rf/MW pulses, and readout window are arranged from top to bottom. rf has a duration of 0.5 μs, while each microwave has a duration corresponding to the π pulse length. (c),(d) ODNMR spectra of $m_s = 0$ (c) and $m_s = -1$ (d) branches at 80 mT. Simulated spectra are shown in the top panels, whereas experimental results are displayed in the bottom panels. Experimental data have been fitted using multiple Lorentz peaks. Inset shows a simplified diagram of the transitions. (e),(f) Magnetic field dependent ODNMR spectra of $m_s = 0$ (e) and $m_s = -1$ (f) branches. Because our diplexer's limited microwave frequency range, the 113 to 134 mT range could not be reached in (f).

Figure 4(c) shows an example of ODNMR spectrum for the transitions within spin sublevels for $|m_s = 0\rangle$ at magnetic field of 80 mT. The rf applied will address the transition between two states and therefore reduce the fluorescence if there is a discrepancy in the brightness of the two states, as shown in inset. This leads to a negative value in the ODNMR contrast, which is calculated as $(\mathrm{signal} - \mathrm{reference})/(\mathrm{signal} + \mathrm{reference})$. Top panel in Fig. 4(c) denotes the transitions as simulated. The simulation result agrees well with the experimental ODNMR spectrum shown in the bottom panel. Similarly, if we apply additional two microwave π pulses, this will allow us to measure the transitions between nuclear spin sublevels for $|m_s = -1\rangle$. Figure 4(d) shows an example for the

transitions for spin sublevels of $|m_s = -1\rangle$. The ODNMR signals below 30 MHz in Fig. 4(d) are attributable to the imperfection of the MW π pulse, which leaves a residual population in the $|m_s = 0\rangle$ state.

The full scan of the ODNMR spectrum as a function of magnetic field is shown in Figs. 4(e) and 4(f). From Fig. 4(e), in the range of 100 to 140 mT, one can see that a larger ODNMR contrast can be achieved when we are approaching the GSLAC point at 128 mT and the linewidth of ODNMR transitions gets broader due to stronger mixing. At exactly 128 mT, we observe a sudden drop in the contrast of the ODNMR spectra. This decrease can be attributed to extensive state mixing between $m_s = 0$ and $m_s = -1$, resulting in reduced electron spin polarization [39]. This is corroborated by our simulation results showcased in Fig. S14. Figure 4(d) showcases the ODNMR results for the $m_s = -1$ branch. Similar conclusions to those previously discussed can be drawn from this data: as the magnetic field enters the range of 100 to 113 mT, and 134 to 140 mT, the transitions noticeably broaden, signifying a high degree of state mixing.

Conclusion.—In summary, we have demonstrated a robust approach for polarizing nuclear spins in h-BN, leveraging the ground-state level anticrossing of V_B^-. Notably, this method can be executed under low-power excitation. The durability of the GSLAC-assisted nuclear polarization is attributable to the extended residence time of ground states in comparison to excited states. Our simulations suggest that an optimized level of nuclear polarization can be attained near a magnetic field strength of 133 mT, where strong state mixing occurs. We emphasize that this GSLAC-assisted nuclear polarization method is broadly applicable and not confined to the specific color center examined in this study. Combined with dynamic decoupling methods to extend the coherence time [42] and the measured coherent rotation of coupled nitrogen nuclear spin results at GSLAC [27], the reliable polarization of nuclear spins in Van der Waals materials has promising implications for quantum sensing technologies and quantum information science, including potential applications in hyperpolarization of samples [43] and quantum registers [44].

S. R., J. K., H. B., X D., F. Z., Y. Z., and W. G. acknowledge Singapore National Research foundation through QEP Grants (NRF2021-QEP2-01-P01, NRF2021-QEP2-01-P02, NRF2021-QEP2-03-P01, NRF2021-QEP2-03-P10, NRF2021-QEP2-03-P11), Agency for Science, Technology and Research Individual Research Grant (M21K2c0116) and Singapore Ministry of Education [MOE2016-T3-1-006 (S)], the Australian Research Council (via CE200100010), and the Asian Office of Aerospace Research and Development Grant No. FA2386-17-1-4064, Office of Naval Research Global (N62909-22-1-2028). F. J. acknowledges the support of Federal Ministry of Education and Research BMBF, ERC (Synergy Grant HyperQ), European Commission (Projects FLORIN, QCIRCLE QuMICRO), DFG (Excellence Cluster POLiS, CRC 1279, and Projects No. 499424854, No. 387073854) and Carl Zeiss Stiftung. H. L. and A. A. B. acknowledge Singapore Ministry of Education (MOE-T2EP50221-0009).

*These authors contributed equally to this letter.
†Contact author: fedor.jelezko@uni-ulm.de
‡Contact author: a.bettiol@nus.edu.sg
§Contact author: wbgao@ntu.edu.sg

[1] Nir Bar-Gill, Linh M. Pham, Andrejs Jarmola, Dmitry Budker, and Ronald L. Walsworth, Solid-state electronic spin coherence time approaching one second, Nat. Commun. **4**, 1743 (2013).

[2] David J. Christle, Abram L. Falk, Paolo Andrich, Paul V. Klimov, Jawad Ul Hassan, Nguyen T. Son, Erik Janzén, Takeshi Ohshima, and David D. Awschalom, Isolated electron spins in silicon carbide with millisecond coherence times, Nat. Mater. **14**, 160 (2015).

[3] Emre Togan, Yiwen Chu, Alexei S. Trifonov, Liang Jiang, Jeronimo Maze, Lilian Childress, M. V. Gurudev Dutt, Anders Søndberg Sørensen, Phillip R. Hemmer, Alexander S. Zibrov, and M. D. Lukin, Quantum entanglement between an optical photon and a solid-state spin qubit, Nature (London) **466**, 730 (2010).

[4] David J. Christle, Paul V. Klimov, Charles F. de las Casas, Krisztián Szász, Viktor Ivády, Valdas Jokubavicius, Jawad Ul Hassan, Mikael Syväjärvi, William F. Koehl, Takeshi Ohshima, Nguyen T. Son, Erik Janzén, Ádám Gali, and David D. Awschalom, Isolated spin qubits in SiC with a high-fidelity infrared spin-to-photon interface, Phys. Rev. X **7**, 021046 (2017).

[5] G. D. Fuchs, Guido Burkard, P. V. Klimov, and D. D. Awschalom, A quantum memory intrinsic to single nitrogen–vacancy centres in diamond, Nat. Phys. **7**, 789 (2011).

[6] Alexandre Bourassa, Christopher P. Anderson, Kevin C. Miao, Mykyta Onizhuk, He Ma, Alexander L. Crook, Hiroshi Abe, Jawad Ul-Hassan, Takeshi Ohshima, Nguyen T. Son, Giulia Galli, and David D. Awschalom, Entanglement and control of single nuclear spins in isotopically engineered silicon carbide, Nat. Mater. **19**, 1319 (2020).

[7] Wei Liu, Nai-Jie Guo, Shang Yu, Yu Meng, Zhi-Peng Li, Yuan-Ze Yang, Zhao-An Wang, Xiao-Dong Zeng, Lin-Ke Xie, Qiang Li, Jun-Feng Wang, Jin-Shi Xu, Yi-Tao Wang, Jian-Shun Tang, Chuan-Feng Li, and Guang-Can Guo, Spin-active defects in hexagonal boron nitride, Mater. Quantum Technol. **2**, 032002 (2022).

[8] Andreas Gottscholl, Matthias Diez, Victor Soltamov, Christian Kasper, Andreas Sperlich, Mehran Kianinia, Carlo Bradac, Igor Aharonovich, and Vladimir Dyakonov, Room temperature coherent control of spin defects in hexagonal boron nitride, Sci. Adv. **7**, eabf3630 (2021).

[9] Xingyu Gao, Boyang Jiang, Andres E. Llacsahuanga Allcca, Kunhong Shen, Mohammad A. Sadi, Abhishek B. Solanki, Peng Ju, Zhujing Xu, Pramey Upadhyaya, Yong P. Chen, Sunil A. Bhave, and Tongcang Li, High-contrast plasmonic-enhanced shallow spin defects in

hexagonal boron nitride for quantum sensing, Nano Lett. **21**, 7708 (2021).

[10] Andreas Gottscholl, Matthias Diez, Victor Soltamov, Christian Kasper, Dominik Krauße, Andreas Sperlich, Mehran Kianinia, Carlo Bradac, Igor Aharonovich, and Vladimir Dyakonov, Spin defects in hBN as promising temperature, pressure and magnetic field quantum sensors, Nat. Commun. **12**, 4480 (2021).

[11] Xiaodan Lyu, Qinghai Tan, Lishu Wu, Chusheng Zhang, Zhaowei Zhang, Zhao Mu, Jesús Zúñiga-Pérez, Hongbing Cai, and Weibo Gao, Strain quantum sensing with spin defects in hexagonal boron nitride, Nano Lett. **22**, 6553 (2022).

[12] Wei Liu, Zhi-Peng Li, Yuan-Ze Yang, Shang Yu, Yu Meng, Zhao-An Wang, Ze-Cheng Li, Nai-Jie Guo, Fei-Fei Yan, Qiang Li, Jun-Feng Wang, Jin-Shi Xu, Yi-Tao Wang, Jian-Shun Tang, Chuan-Feng Li, and Guang-Can Guo, Temperature-dependent energy-level shifts of spin defects in hexagonal boron nitride, ACS Photonics **8**, 1889 (2021).

[13] Mengqi Huang, Jingcheng Zhou, Di Chen, Hanyi Lu, Nathan J. McLaughlin, Senlei Li, Mohammed Alghamdi, Dziga Djugba, Jing Shi, Hailong Wang, and Chunhui Rita Du, Wide field imaging of van der Waals ferromagnet Fe_3GeTe_2 by spin defects in hexagonal boron nitride, Nat. Commun. **13**, 5369 (2022).

[14] A. J. Healey, S. C. Scholten, T. Yang, J. A. Scott, G. J. Abrahams, I. O. Robertson, X. F. Hou, Y. F. Guo, S. Rahman, Y. Lu, M. Kianinia, I. Aharonovich, and J.-P. Tetienne, Quantum microscopy with van der Waals heterostructures, Nat. Phys. **19**, 87 (2023).

[15] Robin Derek Allert, Fleming Bruckmaier, Nick Ruben Neuling, Fabian Alexander Freire-Moschovitis, Kristina Song Liu, Claudia Schrepel, Philip Schätzle, Peter Knittel, Martin Hermans, and Dominik Benjamin Bucher, Microfluidic quantum sensing platform for lab-on-a-chip applications, Lab Chip **22**, 4831 (2022).

[16] Xingyu Gao, Sumukh Vaidya, Kejun Li, Peng Ju, Boyang Jiang, Zhujing Xu, Andres E. Llacsahuanga Allcca, Kunhong Shen, Takashi Taniguchi, Kenji Watanabe, Sunil A. Bhave, Yong P. Chen, Yuan Ping, and Tongcang Li, Nuclear spin polarization and control in hexagonal boron nitride, Nat. Mater. **21**, 1024 (2022).

[17] Jianming Cai, Alex Retzker, Fedor Jelezko, and Martin B. Plenio, A large-scale quantum simulator on a diamond surface at room temperature, Nat. Phys. **9**, 168 (2013).

[18] F. T. Tabesh, M. Fani, J. S. Pedernales, M. B. Plenio, and M. Abdi, Active hyperpolarization of the nuclear spin lattice: Application to hexagonal boron nitride color centers, Phys. Rev. B **107**, 214307 (2023).

[19] V. Jacques, P. Neumann, J. Beck, M. Markham, D. Twitchen, J. Meijer, F. Kaiser, G. Balasubramanian, F. Jelezko, and J. Wrachtrup, Dynamic polarization of single nuclear spins by optical pumping of nitrogen-vacancy color centers in diamond at room temperature, Phys. Rev. Lett. **102**, 057403 (2009).

[20] Andreas Gottscholl, Mehran Kianinia, Victor Soltamov, Sergei Orlinskii, Georgy Mamin, Carlo Bradac, Christian Kasper, Klaus Krambrock, Andreas Sperlich, Milos Toth, Igor Aharonovich, and Vladimir Dyakonov, Initialization and read-out of intrinsic spin defects in a van der Waals crystal at room temperature, Nat. Mater. **19**, 540 (2020).

[21] Pei Yu, Haoyu Sun, Mengqi Wang, Tao Zhang, Xiangyu Ye, Jingwei Zhou, Hangyu Liu, Cheng-Jie Wang, Fazhan Shi, Ya Wang, and Jiangfeng Du, Excited-state spectroscopy of spin defects in hexagonal boron nitride, Nano Lett. **22**, 3545 (2022).

[22] Zhao Mu, Hongbing Cai, Disheng Chen, Jonathan Kenny, Zhengzhi Jiang, Shihao Ru, Xiaodan Lyu, Teck Seng Koh, Xiaogang Liu, Igor Aharonovich, and Weibo Gao, Excited-state optically detected magnetic resonance of spin defects in hexagonal boron nitride, Phys. Rev. Lett. **128**, 216402 (2022).

[23] S. Sangtawesin, C. A. McLellan, B. A. Myers, A. C. Bleszynski Jayich, D. D. Awschalom, and J. R. Petta, Hyperfine-enhanced gyromagnetic ratio of a nuclear spin in diamond, New J. Phys. **18**, 083016 (2016).

[24] C. L. Degen, F. Reinhard, and P. Cappellaro, Quantum sensing, Rev. Mod. Phys. **89**, 035002 (2017).

[25] Jochen Scheuer, Ilai Schwartz, Qiong Chen, David Schulze-Sünninghausen, Patrick Carl, Peter Höfer, Alexander Retzker, Hitoshi Sumiya, Junichi Isoya, and Burkhard Luy, Optically induced dynamic nuclear spin polarisation in diamond, New J. Phys. **18**, 013040 (2016).

[26] Haidong Liang, Yuan Chen, Chengyuan Yang, Kenji Watanabe, Takashi Taniguchi, Goki Eda, and Andrew A. Bettiol, High sensitivity spin defects in hBN created by high-energy He beam irradiation, Adv. Opt. Mater. **11**, 2201941 (2023).

[27] See Supplemental Material at http://link.aps.org/supplemental/10.1103/PhysRevLett.132.266801, which includes Refs. [9,16,22,28–38], for additional information about the experimental methods and a detailed discussion of experimental and simulation results.

[28] Dominik B. Bucher, Diana P. L. Aude Craik, Mikael P. Backlund, Matthew J. Turner, Oren Ben Dor, David R. Glenn, and Ronald L. Walsworth, Quantum diamond spectrometer for nanoscale NMR and ESR spectroscopy, Nat. Protoc. **14**, 2707 (2019).

[29] Francesco Ticozzi and Lorenza Viola, Analysis and synthesis of attractive quantum Markovian dynamics, Automatica **45**, 2002 (2009).

[30] Viktor Ivády, Gergely Barcza, Gergő Thiering, Song Li, Hanen Hamdi, Jyh-Pin Chou, Örs Legeza, and Adam Gali, *Ab initio* theory of the negatively charged boron vacancy qubit in hexagonal boron nitride, npj Comput. Mater. **6**, 1 (2020).

[31] Simon Baber, Ralph Nicholas Edward Malein, Prince Khatri, Paul Steven Keatley, Shi Guo, Freddie Withers, Andrew J. Ramsay, and Isaac J. Luxmoore, Excited state spectroscopy of boron vacancy defects in hexagonal boron nitride using time-resolved optically detected magnetic resonance, Nano Lett. **22**, 461 (2021).

[32] Jeffrey R. Reimers, Jun Shen, Mehran Kianinia, Carlo Bradac, Igor Aharonovich, Michael J. Ford, and Piotr Piecuch, Photoluminescence, photophysics, and photochemistry of the V_B^- defect in hexagonal boron nitride, Phys. Rev. B **102**, 144105 (2020).

[33] Wei Liu, Viktor Ivády, Zhi-Peng Li, Yuan-Ze Yang, Shang Yu, Yu Meng, Zhao-An Wang, Nai-Jie Guo, Fei-Fei Yan, Qiang Li, Jun-Feng Wang, Jin-Shi Xu, Zong-Quan Zhou, Yang Dong, Xiang-Dong Chen, Fang-Wen Sun, Jian-Shun

Tang, Adam Gali, Chuan-Feng Li, and Guang-Can Guo, Coherent dynamics of multi-spin V_B^- center in hexagonal boron nitride, Nat. Commun. **13**, 5713 (2022).

[34] P. London, J. Scheuer, J.-M. Cai, I. Schwarz, A. Retzker, M. B. Plenio, M. Katagiri, T. Teraji, S. Koizumi, J. Isoya, R. Fischer, L. P. McGuinness, B. Naydenov, and F. Jelezko, Detecting and polarizing nuclear spins with double resonance on a single electron spin, Phys. Rev. Lett. **111**, 067601 (2013).

[35] D. Farfurnik, Y. Horowicz, and N. Bar-Gill, Identifying and decoupling many-body interactions in spin ensembles in diamond, Phys. Rev. A **98**, 033409 (2018).

[36] Katharina Senkalla, Genko Genov, Mathias H. Metsch, Petr Siyushev, and Fedor Jelezko, Germanium vacancy in diamond quantum memory exceeding 20 ms, Phys. Rev. Lett. **132**, 026901 (2024).

[37] A. Jarmola, I. Fescenko, V. M. Acosta, M. W. Doherty, F. K. Fatemi, T. Ivanov, D. Budker, and V. S. Malinovsky, Robust optical readout and characterization of nuclear spin transitions in nitrogen-vacancy ensembles in diamond, Phys. Rev. Res. **2**, 023094 (2020).

[38] Shimon Kolkowitz, Quirin P. Unterreithmeier, Steven D. Bennett, and Mikhail D. Lukin, Sensing distant nuclear spins with a single electron spin, Phys. Rev. Lett. **109**, 137601 (2012).

[39] Xing-Fei He, Neil B. Manson, and Peter T. H. Fisk, Paramagnetic resonance of photoexcited N-V defects in diamond. II. Hyperfine interaction with the ^{14}N nucleus, Phys. Rev. B **47**, 8816 (1993).

[40] A. Wokaun and Richard R. Ernst, Selective detection of multiple quantum transitions in NMR by two-dimensional spectroscopy, Chem. Phys. Lett. **52**, 407 (1977).

[41] V. W. Hughes and J. S. Geiger, Two-quantum transitions in the microwave Zeeman spectrum of atomic oxygen, Phys. Rev. **99**, 1842 (1955).

[42] Roberto Rizzato, Martin Schalk, Stephan Mohr, Jens C. Hermann, Joachim P. Leibold, Fleming Bruckmaier, Giovanna Salvitti, Chenjiang Qian, Peirui Ji, Georgy V. Astakhov, Ulrich Kentsch, Manfred Helm, Andreas V. Stier, Jonathan J. Finley, and Dominik B. Bucher, Extending the coherence of spin defects in hBN enables advanced qubit control and quantum sensing, Nat. Commun. **14**, 5089 (2023).

[43] David R. Glenn, Dominik B. Bucher, Junghyun Lee, Mikhail D. Lukin, Hongkun Park, and Ronald L. Walsworth, High-resolution magnetic resonance spectroscopy using a solid-state spin sensor, Nature (London) **555**, 351 (2018).

[44] M. V. Gurudev Dutt, L. Childress, L. Jiang, E. Togan, J. Maze, F. Jelezko, A. S. Zibrov, P. R. Hemmer, and M. D. Lukin, Quantum register based on individual electronic and nuclear spin qubits in diamond, Science **316**, 1312 (2007).